Marquette University
e-Publications@Marquette

Chemistry Faculty Research and Publications | Chemistry, Department of

2013

Frozen Rotor Approximation in the Mixed Quantum/Classical Theory for Collisional Energy Transfer: Application to Ozone Stabilization

Alexander Teplukhin
Marquette University

Mikhail V. Ivanov
Marquette University

Dmitri Babikov
Marquette University, dmitri.babikov@marquette.edu

Follow this and additional works at: https://epublications.marquette.edu/chem_fac

 Part of the Chemistry Commons

Recommended Citation

Teplukhin, Alexander; Ivanov, Mikhail V.; and Babikov, Dmitri, "Frozen Rotor Approximation in the Mixed Quantum/Classical Theory for Collisional Energy Transfer: Application to Ozone Stabilization" (2013). *Chemistry Faculty Research and Publications*. 274.
https://epublications.marquette.edu/chem_fac/274

Frozen rotor approximation in the mixed quantum/classical theory for collisional energy transfer: Application to ozone stabilization

Alexander Teplukhin, Mikhail Ivanov, and Dmitri Babikov[a)]
Chemistry Department, Wehr Chemistry Building, Marquette University, Milwaukee, Wisconsin 53201-1881, USA

(Received 8 July 2013; accepted 2 September 2013; published online 23 September 2013)

A frozen-rotor approximation is formulated for the mixed quantum/classical theory of collisional energy transfer and ro-vibrational energy flow [M. Ivanov and D. Babikov, J. Chem. Phys. **134**, 144107 (2011)]. Numerical tests are conducted to assess its efficiency and accuracy, compared to the original version of the method, where rotation of the molecule in space is treated explicitly and adiabatically. New approach is considerably faster and helps blocking the artificial ro-vibrational transitions at the pre- and post-collisional stages of the process. Although molecular orientation in space is fixed, the energy exchange between rotational, vibrational, and translational digresses of freedom still occurs, allowing to compute ro-vibrational excitation and quenching. Behavior of the energy transfer function through eight orders of magnitude range of values and in a broad range of ΔE is reproduced well. In the range of moderate $-500 \le \Delta E \le +500\,\mathrm{cm}^{-1}$ the approximate method is rather accurate. The absolute values of stabilization cross sections for scattering resonances trapped behind the centrifugal threshold are a factor 2-to-3 smaller (compared to the explicit-rotation approach). This performance is acceptable and similar to the well-known sudden-rotation approximation in the time-independent inelastic scattering methods. © *2013 AIP Publishing LLC*. [http://dx.doi.org/10.1063/1.4821349]

I. INTRODUCTION

Collisional energy transfer (CET) plays crucial role during the second step of the recombination reaction that forms ozone in Earth's atmosphere:

$$O + O_2 \leftrightarrow O_3{}^*, \tag{1}$$

$$O_3{}^* + M \rightarrow O_3 + M^*. \tag{2}$$

Here, M can be any atmospheric molecule (or Ar atom in laboratory experiments[1]), whose role is to remove energy from the metastable $O_3{}^*$ states (excited ro-vibrationally above the dissociation threshold) to produce stable ozone molecules, O_3. In order to provide complete theoretical treatment of ozone formation kinetics one should be able, ideally, to compute cross sections for all ro-vibrational state-to-state transitions that take place in $O_3{}^*$ due to collisions with M, and incorporate those data into the master equation formalism.[2,3] While very easy to state, this is practically impossible to do. The density of vibrational states near dissociation threshold of ozone is close to one state per 1.2 cm^{-1}, and each of those vibrational states is accompanied by a dense spectrum of rotational states (rotational constant is ~0.4 cm^{-1}). Ozone is a heavy rotor and a broad distribution of rotational states (up to $J \sim 90$) is populated at room temperature. Thus, the rotational transitions between different J-values are impossible to rule out. Rotational energy transfer occurs simultaneously with vibrational stabilization and plays a very important role. Moreover, the collision-induced dissociation (CID) of $O_3{}^*$ takes place simultaneously with its stabilization and should also be described theoretically.

The classical-trajectory treatment of process (2) was relatively straightforward,[4] but it did not help to answer questions related to the famous anomalous isotope effect,[1,5] which is believed to be related to quantum mechanical phenomena such as zero-point energy, symmetry, and scattering resonances.[6–8] On the other extreme side, the full-fledged quantum treatment of the process is unaffordable computationally, for the reasons discussed in the previous paragraph (large density of states, importance of rotational excitation, dissociation). Thus, several theory groups searched for alternatives to the exact quantum mechanics. The first *approximate* quantum treatment of process (2) was proposed by Clary's group within the time-independent coupled-channel formalism.[9,10] They used the dimensionally reduced model of ozone (frozen bending) and looked at non-rotating ozone molecule ($J = 0$ only). The next study by Bowman's group[11] offered a considerable improvement through implementing the full-dimensional treatment of O_3^*. However, their calculations have been carried out for very few (just three) collision geometries of $M + O_3^*$. A similar treatment was developed by Schinke's group,[12,13] also based on the coupled-channel formalism for $J = 0$. Their calculations converged with respect to the number of partial waves for orbital motion, but their basis set contained just the bound states of O_3 (below dissociation threshold) so, no metastable states of O_3^* (scattering resonances above dissociation threshold) were involved at all. Neither of these groups incorporated lifetimes of O_3^* into their treatment of kinetics.

Recently, the group of Babikov implemented a conceptually different method for theoretical treatment of the ozone forming reaction—the mixed quantum/classical

a)Author to whom correspondence should be addressed. Electronic mail: dmitri.babikov@mu.edu

 © 2013 AIP Publishing LLC

theory (MQCT) for collisional energy transfer and ro-vibrational energy flow.[14] This method is still approximate, but it overcomes many difficulties encountered earlier by other workers. Namely, the scattering of M and the rotational quenching of O_3^* are treated classically, which allows covering a broad range of rotational excitations, up to $J \sim 90$. These classical approximations are well justified because no quantum effects are expected to occur due to scattering of heavy M, or due to rotation of heavy O_3^*. The vibrational motion of ozone, however, is treated with time-dependent Schrödinger equation, which incorporates zero-point energy and vibrational symmetry. The scattering resonances of O_3^* are also accessible, including quantization of their energies, accurate calculations of their decay rates and CID.[15,16]

The MQCT is computationally feasible (in contrast to the full-quantum methods) but the high density of vibrational states and the broad range of rotational excitations in ozone make even these calculations highly demanding. For these reasons, the calculations of Babikov's group were carried out within the dimensionally reduced model of ozone,[14,17] where only two bond stretches were treated explicitly, while the bending motion was treated adiabatically (relaxed).

There is a strong need to progress towards the full-dimensional treatment of ozone formation, including its bending motion. Moreover, oxygen has three stable isotopes, which results in as many as 36 isotopically different versions of the processes (1) and (2)[1] and all of those should, ideally, be explored theoretically! In order to make such calculations computationally affordable one should think of some additional simplifications, within the framework of MQCT.

In this paper we formulate and test the frozen-rotation (FR) approximation for MQCT. Since MQCT is time-dependent and involves classical as well as quantum degrees of freedom, the approximation we devise here is very different from the well-known sudden-rotation approximation used in the time-independent full-quantum calculations.[18–21] The main purpose of our FR approximation is to "freeze" the rotation of O_3^* during the $M + O_3^*$ scattering event, *without* cutting off the energy exchange between translational, rotational, and vibrational degrees of freedom. Freezing the rotation of O_3^* gives significant computational advantages (discussed in the paper), with relatively small intervention into the energy exchange process. Interestingly, it appears that rotational excitation and/or quenching of the molecule can be described without letting the molecule rotate in space during the collision with M.

The paper is organized as follows. The MQCT method is briefly reviewed in Sec. II. The formalism of FR approximation is introduced in Sec. III. Numerical results that serve as a test of accuracy of the FR approximation are presented and discussed in Sec. IV. Section V summarizes all the work done.

II. THE MIXED QUANTUM/CLASSICAL THEORY

The idea of mixed quantum/classical treatment of collisional energy transfer is not entirely new.[22–26] A good review of methods and their applications was done by Billing.[27] In our implementation of MQCT[14] the vibrational motion of oxygen atoms in O_3 is treated quantum mechanically, while the rotational motion of O_3 and the translational (scattering) motion of $Ar + O_3$ are treated classically. All coordinates are divided into two groups: those describing quantum part of the system and those describing classical part. The former set is internal bond-angle coordinates $\mathbf{R}_Q = (R_1, R_2, \theta)$. The latter set $\mathbf{R}_C = (\mathbf{q}_{O_3}, \mathbf{q}_{Ar}, \alpha, \beta, \gamma)$ includes the Cartesian coordinates of ozone $\mathbf{q}_{O_3}$ and quencher $\mathbf{q}_{Ar}$ in the laboratory-fixed frame and Euler angles (α, β, γ) for orientation of O_3 molecule in space.

Quantum description of vibrational motion involves propagation of wave function $\Psi(\mathbf{R}_Q,t)$ using the time-dependent Schrödinger equation:

$$i\frac{\partial}{\partial t}\Psi(\mathbf{R}_Q, t) = \hat{H}(t)\Psi(\mathbf{R}_Q, t,) \tag{3}$$

$$\hat{H}(t) = \hat{T}_{J=0} + V(\mathbf{R}_Q;\ \mathbf{R}_C(t)) + V_{rot}(\mathbf{R}_Q;\ \mathbf{R}_C(t)). \tag{4}$$

Through the $V(\mathbf{R}_Q;\ \mathbf{R}_C(t))$ dependence of the PES, the classical trajectory of motion $\mathbf{R}_C(t)$ affects evolution of the quantum part of the system (vibration). The effect of rotational motion on vibration is included adiabatically,[28–33] by introducing into the Hamiltonian of Eq. (4) the rotational potential V_{rot}, which is a smooth function of coordinates, computed numerically on a grid of points in $\mathbf{R}_Q$ using

$$V_{rot}(\mathbf{R}_Q) = \tfrac{1}{2}(\mathbf{J}, \mathbf{I}^{-1}(\mathbf{R}_Q)\mathbf{J}). \tag{5}$$

Here, $\mathbf{I}(\mathbf{R}_Q)$ is the tensor of inertia on the grid and $\mathbf{J}(t)$ is the instantaneous vector of angular momentum of the molecule, both expressed in the lab reference frame. Rotational potential is a time dependent quantity.

The rotation itself is treated classically using the *fluid-rotor* equations of motion:[14]

$$\begin{pmatrix}\ddot{\alpha}\\ \ddot{\beta}\\ \ddot{\gamma}\end{pmatrix} = \mathbf{G}^{-1}\left[\tilde{\mathbf{I}}^{-1}\left[\tilde{\boldsymbol{\tau}} - \dot{\tilde{\mathbf{I}}}\mathbf{G}\begin{pmatrix}\dot{\alpha}\\ \dot{\beta}\\ \dot{\gamma}\end{pmatrix}\right] - \dot{\mathbf{G}}\begin{pmatrix}\dot{\alpha}\\ \dot{\beta}\\ \dot{\gamma}\end{pmatrix}\right]. \tag{6}$$

Here, $\tilde{\mathbf{I}}(t)$ is the instantaneous mean tensor of inertia of the fluid rotor, while $\tilde{\boldsymbol{\tau}}(t)$ is the mean torque on the molecule (caused by the quencher), defined as

$$\tilde{\mathbf{I}} = \langle\Psi(\mathbf{R}_Q, t)|\ \mathbf{I}^{-1}(\mathbf{R}_Q)|\Psi(\mathbf{R}_Q, t)\rangle^{-1}, \tag{7}$$

$$\tilde{\boldsymbol{\tau}} = -\langle\Psi(\mathbf{R}_Q)|\sum_i \mathbf{r}_i \times \nabla V|\Psi(\mathbf{R}_Q)\rangle, \tag{8}$$

where $\mathbf{r}_i = \{x_i, y_i, z_i\}$ is the radius vector of ith atom relative to molecular center or mass, $\mathbf{r}_i \times \nabla V$ represents the torque of the quencher on ith atom in the molecule, and the gradient ∇V is computed with respect to the Cartesian position of ith atom. Summation in Eq. (8) is over three O atoms. Matrix $\mathbf{G}$ in Eq. (6) was introduced for convenience:

$$\mathbf{G} = \begin{pmatrix}0 & \cos\alpha & \sin\beta\sin\alpha\\ 0 & \sin\alpha & -\sin\beta\cos\alpha\\ 1 & 0 & \cos\beta\end{pmatrix}. \tag{9}$$

Time derivative $\dot{\tilde{\mathbf{I}}}$ in Eq. (6) is computed as $\dot{\tilde{\mathbf{I}}} = \tilde{\mathbf{I}}\mathbf{A}\tilde{\mathbf{I}}$, where matrix $\mathbf{A}$ is

$$\mathbf{A} = \langle\Psi|\ \mathbf{I}^{-1}\left(\frac{d\mathbf{I}}{dt}\right)\ \mathbf{I}^{-1}\ |\Psi\rangle - 2\ \mathrm{Re}\langle\Psi|\ \mathbf{I}^{-1}\left|\frac{d}{dt}\Psi\right\rangle. \quad (10)$$

Note that evolution of the vibrational state of the system affects its classical rotational motion, through vibrational wave function $\Psi(\mathbf{R}_\mathrm{Q}, t)$ in expressions for the mean values of $\tilde{\mathbf{I}}$, $\tilde{\boldsymbol{\tau}}$, and $\mathbf{A}$.

Translational coordinates $\mathbf{q}_{\mathrm{O}_3}$ and $\mathbf{q}_{\mathrm{Ar}}$ are propagated using classical equations of motion: $\dot{\mathbf{q}} = \mathbf{p}/M$ and $\dot{\mathbf{p}} = -\nabla\tilde{V}$, where transcripts are omitted for simplicity, and the mean field potential is defined as

$$\tilde{V}(\mathbf{R}_C, t) = \langle\Psi(\mathbf{R}_\mathrm{Q}, t)|V(\mathbf{R}_\mathrm{Q}; \mathbf{R}_C(t))|\Psi(\mathbf{R}_\mathrm{Q}, t)\rangle. \quad (11)$$

Again, quantum vibrational state of the system $\Psi(\mathbf{R}_\mathrm{Q}, t)$ influences the classical trajectory for scattering, through $\tilde{V}$.

Overall, the energy is exchanged between translation, rotation, and vibration, while the total energy is conserved.

III. FROZEN ROTOR APPROXIMATION

Let us start from the formal side of implementing the frozen-rotor approximation. Two terms in Eq. (10) have very transparent physical meaning. The first term is a rigid-rotor term, while the second term is a fluid-rotor term. The second term is zero if the vibrational wave function $\Psi(\mathbf{R}_\mathrm{Q})$ is constant over the time. Its effect on rotation becomes important only if the vibrational motion occurs and the wave function changes, which affects the tensor of inertia. We want to keep this term, because it describes ro-vibrational interaction. The first term in Eq. (10) is a simple rotation in 3D of the tensor of inertia of the rigid body. If the molecule does not rotate, this term is unnecessary. So, in the frozen-rotor case Eq. (10) simplifies to

$$\mathbf{A} = -2\ \mathrm{Re}\langle\Psi(\mathbf{R}_\mathrm{Q})|\ \mathbf{I}^{-1}(\mathbf{R}_\mathrm{Q})\left|\frac{d}{dt}\Psi(\mathbf{R}_\mathrm{Q})\right\rangle. \quad (12)$$

Note that our frozen rotor remains fluid, due to the time derivative in Eq. (12). Within its original orientation in space, the tensor of inertia is allowed to change over the time if $d\Psi\,/\,dt \neq 0$, for example, due to centrifugal effect or due to interaction with quencher.

Furthermore, if molecule does not rotate, its orientation in space is constant and $\dot{\mathbf{G}} = 0$. So, the last term in Eq. (6) vanishes. Now it is convenient to introduce $\upsilon_\alpha = \dot{\alpha}$, $\upsilon_\beta = \dot{\beta}$, and $\upsilon_\gamma = \dot{\gamma}$. These moieties are related to angular velocity $\boldsymbol{\omega}$ through

$$\boldsymbol{\omega} = \mathbf{G}\begin{pmatrix}\upsilon_\alpha\\ \upsilon_\beta\\ \upsilon_\gamma\end{pmatrix}. \quad (13)$$

In these notations, Eq. (6) can be rewritten as follows:

$$\begin{pmatrix}\dot{\alpha}\\ \dot{\beta}\\ \dot{\gamma}\end{pmatrix} = \begin{pmatrix}\upsilon_\alpha\\ \upsilon_\beta\\ \upsilon_\gamma\end{pmatrix}, \quad (14)$$

$$\begin{pmatrix}\dot{\upsilon}_\alpha\\ \dot{\upsilon}_\beta\\ \dot{\upsilon}_\gamma\end{pmatrix} = \mathbf{G}^{-1}\left[\tilde{\mathbf{I}}^{-1}\left[\tilde{\boldsymbol{\tau}} - \frac{d\tilde{\mathbf{I}}}{dt}\mathbf{G}\begin{pmatrix}\upsilon_\alpha\\ \upsilon_\beta\\ \upsilon_\gamma\end{pmatrix}\right]\right]. \quad (15)$$

If the molecule does not rotate in space, we do not have to propagate Eq. (14) for angles at all, equivalent to saying that $\dot{\alpha} = 0$, $\dot{\beta} = 0$, and $\dot{\gamma} = 0$. Only Eq. (15) should be propagated. It captures the effect of rotational excitation and/or quenching and emphasizes that our frozen-rotor remains fluid, within its original orientation in space. If the mean tensor of inertia changes, $d\tilde{\mathbf{I}}/dt \neq 0$, its effect onto rotational excitation is included.

The existing computer code[14] can be very easily modified to propagate Eqs. (12) and (15), instead of Eqs. (6) and (10). Note, however, that Eq. (15) can be conveniently rewritten using Eq. (13) as follows:

$$\dot{\boldsymbol{\omega}} = \tilde{\mathbf{I}}^{-1}\left[\tilde{\boldsymbol{\tau}} - \frac{d\tilde{\mathbf{I}}}{dt}\boldsymbol{\omega}\right]. \quad (16)$$

Rearranging terms, using chain rule and introducing angular momentum $\mathbf{J} = \tilde{\mathbf{I}}\omega$ we obtain

$$\frac{d\mathbf{J}}{dt} = \tilde{\boldsymbol{\tau}}. \quad (17)$$

Indeed, if the molecule is forcedly fixed in space, no equations for rotational coordinates are necessary at all. All we have to do is to integrate torque $\tilde{\boldsymbol{\tau}}(t)$ due to quencher along the trajectory to determine the change of $\mathbf{J}$ (i.e., rotational excitation or quenching). The time dependent value of $\mathbf{J}(t)$ goes directly into Eq. (5) to give evolution of rotational potential $V_\mathrm{rot}(\mathbf{R}_\mathrm{Q})$ along the trajectory $\mathbf{R}_C(t)$ for inclusion into the Hamiltonian of Eq. (4). This is almost embarrassingly simple, but makes sense.

IV. RESULTS AND DISCUSSION

We carried out preliminary calculations using both versions: either propagating Eqs. (12) and (15) or, alternatively, Eq. (17) alone. The results are entirely identical, however, Eq. (17) gives significant computational advantage, since calculations of the wave function derivative $d\Psi\,/\,dt$ (on the grid) in Eq. (12) are avoided, as well as numerous matrix operations in Eq. (15). The computational advantage of the FR method is substantial, speedup by a factor of $\times 3.8$.

A. Examples of a single trajectory

Details of setting up the initial conditions for MQCT calculations have already been discussed in detail.[14] Initial wave function is one of vibrational eigenstates in the rotationally excited potential: $\Psi(\mathbf{R}_\mathrm{Q}, t_0) = \Phi_n^{(i)}(\mathbf{R}_\mathrm{Q})$. Here, index i denotes initial rotational excitation (quantized semi-classically), while index n denotes a vibrational state in this rotationally excited potential. We always start at a scattering resonance, namely, the ro-vibrational state above the dissociation threshold, $E_n^{(i)} > 0$. The vibrational spectrum of $^{16}\mathrm{O}^{18}\mathrm{O}^{16}\mathrm{O}$ in the dimensionally reduced model is relatively sparse. The upper part of spectrum, within the energy range $\sim$1000 cm^{-1} below

TABLE I. Cross sections (a_0^2) for vibrational state-to-state transitions and stabilization of the normal mode state (#51).

Final vibrational state		Initial rotational state[a]							
		$J = 25, K = 5$ (73.4; 3.5×10^{-5})		$J = 35, K = 0$ (241.1; 1.1×10^{-4})		$J = 35, K = 5$ (309.0; 1.9×10^{-3})		$J = 35, K = 12$ (629.9; 1.5×10^{-3})	
#	Character	AR	FR	AR	FR	AR	FR	AR	FR
51	N	422.898	473.141	417.682	479.024	416.552	473.649	402.366	460.521
50	L2	0.100	0.085	0.139	0.057	0.120	0.079	0.202	0.376
49	L1	0.095	0.057	0.091	0.044	0.111	0.058	0.277	0.035
48	N	3.316	1.130	4.345	1.014	5.407	1.106	9.460	1.313
47	L2	0.030	0.034	0.046	0.018	0.036	0.032	0.174	0.074
46	L1	0.028	0.018	0.027	0.018	0.036	0.014	0.118	0.022
45	N	0.086	0.028	0.133	0.025	0.198	0.029	0.508	0.029
44	N	0.003	0.002	0.004	0.002	0.007	0.002	0.016	0.003
43	N	0.002	0.001	0.002	0.001	0.003	0.001	0.011	0.002
42	L2	0.003	0.000	0.000	0.000	0.000	0.000	0.001	0.002
41	L1	0.000	0.000	0.000	0.000	0.000	0.000	0.000	0.000
Ro-vibrational stabilization		99.969	47.206	51.375	26.318	45.481	14.620	10.430	3.439

[a]Each scattering resonance is characterized by J, K, energy and width (in parenthesis) in the units of wave number.

the dissociation threshold, contains only 11 vibrational states (#41 to 51 in Tables I and II). Some of them belong to progression of the normal vibration modes (labeled by N), and some to the local-vibration mode progression associated with either channel 1 or 2 (namely, O–OO or OO–O, labeled L1 and L2). Typical rotational excitations of $J \sim$ 20-45 bring these states up (the centrifugal effect) and converts them into scattering resonances trapped behind the centrifugal barrier at energies few hundred wavenumbers above the dissociation threshold. These are our initial states. Note that in rotationally excited ozone the vibrational motion is rather localized, due to sharp centrifugal barrier. We found that in such conditions all vibrational states can be easily assigned (in terms of quantum numbers) up to dissociation threshold and even above. This is very different from the non-rotating ozone, where the upper 20% of vibrational spectrum exhibit irregular behavior due to flattening of the PES near dissociation threshold.[34–37]

In Fig. 1 we consider an example trajectory which starts at the scattering resonance with $J = 35$ and $K = -5$, $n = 50$ and $E_n^{(i)} = 133.6$ cm^{-1} (specifying semi-classical initial conditions for rotation we set $K_b = K_c$ and assume that $K = K_a$ is good quantum number, for simplicity). This is a local-mode state with 8 quanta of vibration along the $O + O_2$ dissociation channel and one quantum of vibration in O_2. Collision energy of Ar is $E_{\rm coll} = 217$ cm^{-1} and impact parameter is $b = 3.64\, a_0$. Plotted in Fig. 1 are the values of rotational potential $V_{\rm rot}(\mathbf{R}_{\rm Q})$ at two important points on the PES: the bottom of covalent well (Fig. 1(a)) and the top of centrifugal barrier in one of

TABLE II. Cross sections (a_0^2) for vibrational state-to-state transitions and stabilization of the local mode state (#50).

Final vibrational state		Initial rotational state[a]							
		$J = 20, K = 9$ (26.1; 3.8×10^{-6})		$J = 35, K = -5$ (133.6; 8.7×10^{-3})		$J = 35, K = 9$ (349.7; 2.5×10^{-6})		$J = 45, K = -5$ (418.6; 2.5×10^{-1})	
#	Character	AR	FR	AR	FR	AR	FR	AR	FR
51	N	0.077	0.083	0.143	0.039	0.911	0.074	0.374	0.012
50	L2	400.088	434.582	365.551	359.478	360.393	427.081	360.987	244.492
49	L1	0.668	0.728	1.651	1.808	1.390	0.236	0.576	0.744
48	N	0.776	2.395	11.430	18.729	2.451	4.340	5.623	3.137
47	L2	29.544	16.832	41.678	8.661	33.814	15.381	41.652	5.309
46	L1	0.078	0.211	0.289	0.620	0.902	0.125	0.232	0.257
45	N	0.639	0.638	1.890	1.049	3.730	0.587	3.098	1.161
44	N	0.026	0.172	0.029	0.234	0.372	0.068	0.048	0.207
43	N	0.026	0.028	0.018	0.041	0.360	0.021	0.048	0.022
42	L2	0.016	0.070	0.017	0.020	0.332	0.077	0.040	0.016
41	L1	0.005	0.004	0.000	0.014	0.128	0.003	0.015	0.012
Ro-vibrational stabilization		127.245	94.858	104.177	52.552	45.906	14.148	48.544	18.438

[a]Each scattering resonance is characterized by J, K, energy and width (in parenthesis) in the units of wave number.

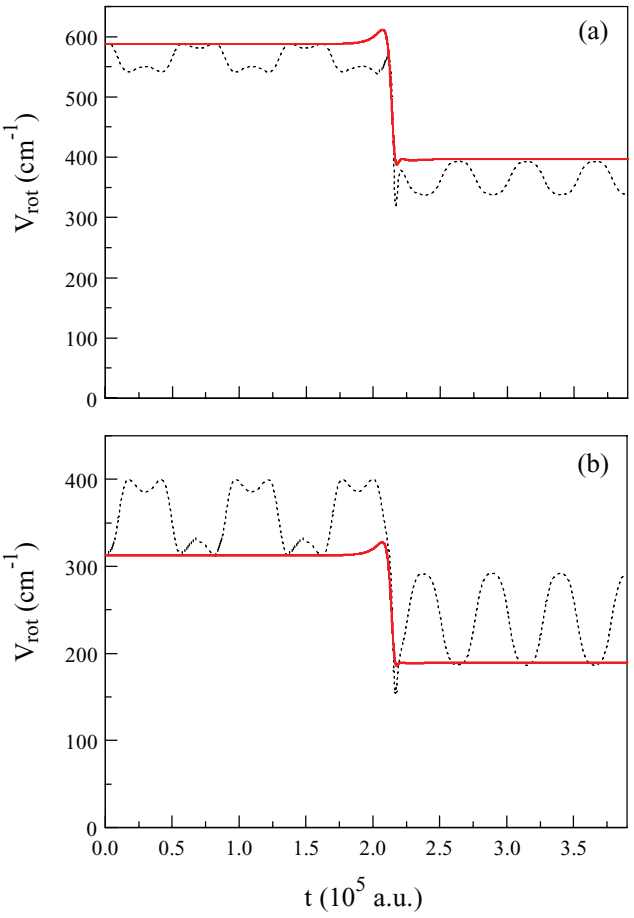

FIG. 1. Time evolution of rotational potential along one trajectory at the point near (a) bottom of covalent well on the PES of ozone $R_1 = R_2 = 2.4\ a_0$; (b) top of centrifugal barrier $R_1 = 2.3\ a_0$, $R_2 = 3.8\ a_0$. Red solid line stands for FR-method, black dotted stands for AR-method. Initial (classical) rotational state is $J = 35$, $K = -5$, and the ro-vibrational energy is $E_n^{(i)} = 133.6$ cm^{-1}. See text for further details.

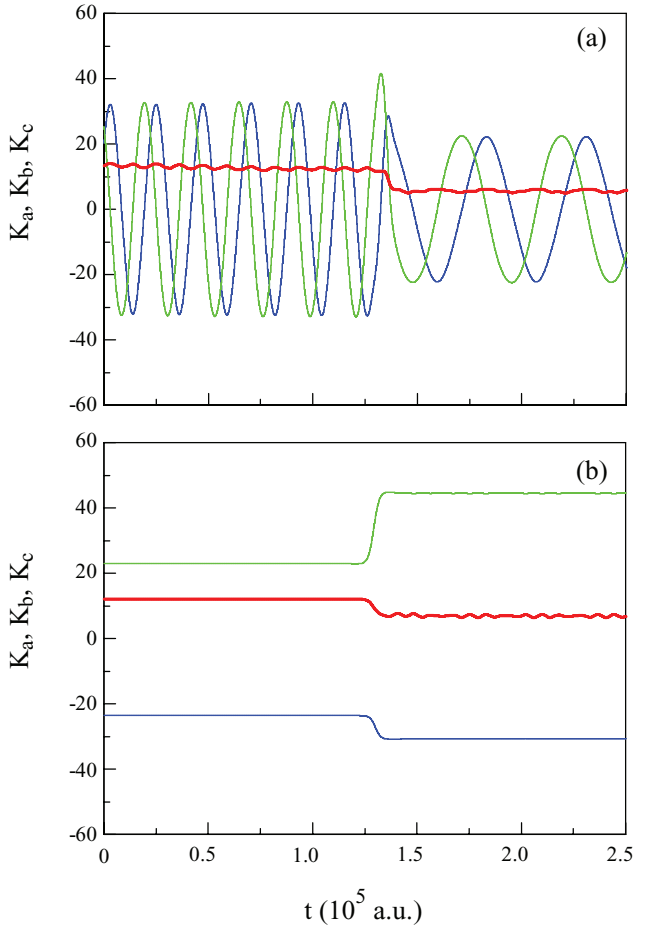

FIG. 2. Time evolution of K_a (red), K_b and K_c (blue and green) along a typical trajectory for initial $J = 35$, $K_a = 12$, $|K_b| = |K_c| = 23$ and vibrational state $n = 50$. (a) Original AR method; (b) developed FR approach. One sees that K_a is approximately a good quantum number in both cases.

the dissociation channels (Fig. 1(b)). We can see that in the original MQCT method, where the adiabatic-rotation (AR) is explicitly going on, the centrifugal potential V_{rot} evolves during the pre-collisional and post-collisional stages of the process, due to the ro-vibrational interaction in the fluid rotor model. In the frozen-rotor version of MQCT the rotational potential $V_{rot}(\mathbf{R}_Q)$ is constant over time (at every point of the $\mathbf{R}_Q$ grid). Note that for description of the resonance stabilization, for CET, the focus is not really on the ro-vibrational interaction during the pre- and post-collisional stages, but more on the molecule-quencher interaction during the short collision event. Figure 1 demonstrates that this last effect is well described by the FR approximation.

In the time-dependent mixed quantum/classical method we do not really have to make any assumptions about goodness of the rotational quantum number K, because we use classical trajectories for description of rotation, either as fluid-rotor or as rigid-rotor. In either case, three components of J evolve during the dynamics. Figure 2(a) shows an example of typical trajectory ($b = 2.55\ a_0$ and $E_{coll} = 489$ cm^{-1}) for the initial vibrational state $n = 50$ and a quasi-classical initial state $J = 35$, $K = K_a = 12$, $|K_b| = |K_c| = 23$. One sees that the value of K_a is approximately conserved on the pre-collisional and post-collisional stages, in contrast to K_b and K_c that oscillate widely. This picture supports a well-known fact—ozone is very close to a symmetric top. Its rotational constants are only ~10% different. For simplicity, we sample the initial rotational states such that $|K_b| = |K_c|$, so that we can label these quasi-classical initial conditions by J and K only. As rotation starts (on the pre-collisional stage) the memory of $|K_b| = |K_c|$ is immediately lost, while $K = K_a$ remains roughly the same. Figure 2(b) demonstrates that K remains good quantum number in the FR-method too.

One more advantage given by the FR approximation becomes obvious. On the post collisional stage the centrifugal potential is constant, so, one can start spectral analysis of the final vibrational wave packet $\Psi(\mathbf{R}_Q, t_{fin})$ at any moment of time, as soon as quencher leaves. This is not so straightforward in the AR version of the method, where rotational potential continues evolving due to ongoing ro-vibrational interaction. This continuing ro-vibrational energy exchange causes artificial ro-vibrational transitions at the post-collisional stage, which is a known deficiency of the mixed quantum/classical treatment.[14] In order to cancel its effect we usually use the forward-backward propagation technique,[38] but it doubles the computational effort. In the FR version of MQCT this problem does not exist, so that the

backward propagation is unnecessary, which saves computational resources.

B. Energy transfer

Projection onto vibrational eigenstates of the final rotational potential permits to compute energy spectrum of the final wave packet, or the probabilities of state-to-state transitions:

$$p^{(i)}_{n,n'} = \left|\left\langle \Phi^{(i')}_{n'}(\mathbf{R}_Q) \,\middle|\, \Psi(\mathbf{R}_Q, t_{fin})\right\rangle\right|^2. \quad (18)$$

This information, together with magnitudes of the energy transfer $\Delta E = E^{(i')}_{n'} - E^{(i)}_{n}$, can be used to bin the data for a batch of trajectories into a 2D-histogram, like those presented in Fig. 3 (3000 trajectories for the same initial state as Fig. 1).

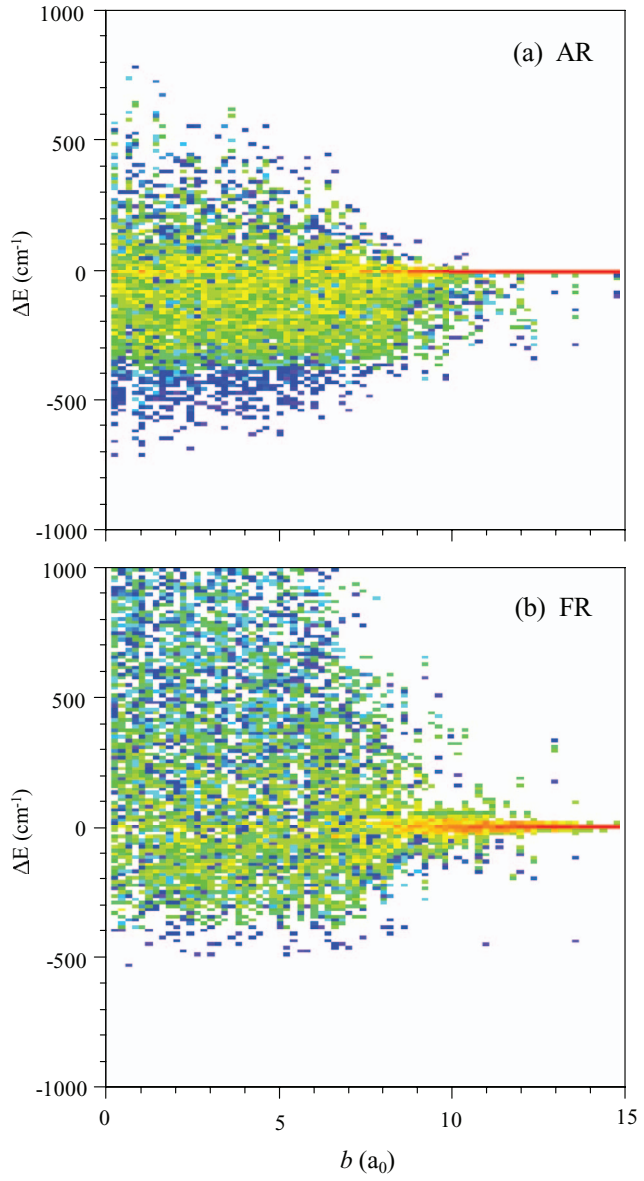

FIG. 3. Intensity of the energy transfer as a function of impact parameter b and the magnitude of energy change ΔE for a batch of 3000 trajectories in the (a) original AR method; (b) developed FR approach. Red is for high intensity, blue is for low intensity. Excitation is at positive ΔE, quenching is at negative ΔE. Elastic peak is at $\Delta E = 0$ and large impact parameter. Initial ro-vibrational state is the same as in Fig. 1.

These plots visualize intensity of the excitation/quenching as a function of impact parameter $0 \le b \le 15\ a_0$ and the magnitude of energy transfer $-1000 \le \Delta E \le +1000\,\mathrm{cm}^{-1}$. Collision energy was sampled from thermal distribution at room temperature. Figure 3(a) describes the case of explicit adiabatic rotation, while Fig. 3(b) corresponds to our frozen-rotor approach . Both methods show the elastic scattering peak ($\Delta E = 0$) at large impact parameters, and both indicate quenching ($\Delta E < 0$) as well as excitation ($\Delta E > 0$) going on at impact parameters less than $b \approx 8\ a_0$. We have to admit that in the FR case the excitation is clearly overestimated in the region of $\Delta E > +500\ \mathrm{cm}^{-1}$, compared to the AR case. Explanation is as follows: when the rotational motion is frozen, the ability of the molecule to dodge the quencher is limited to the translational recoil only, which leads to more intense interaction with quencher and larger amount of energy is transferred to the molecule. This is a negative consequence of FR approximation.

It should also be mentioned that the total energy in the FR method is not exactly conserved. We conducted a careful study of this issue and found that for some trajectories the total energy increases as a result of collision, while it decreases for others. Average over the batch of trajectories, with thermal distribution of collision energies at room temperature, leads to relatively small overall energy defect.

The weighted sum over b of the 2D-histogram in Fig. 3 produces a differential (over ΔE) cross section for energy transfer, plotted in Fig. 4. Such dependence is used in analytic theories of CET[39–41] and is sometimes called the energy transfer function. Comparison of the AR *vs.* FR data (filled *vs.* empty symbols) shows that in the regime of moderate energy transfer, $-500 \le \Delta E \le +500\,\mathrm{cm}^{-1}$, the agreement between two methods is reasonably good. Furthermore, the overall trend of the differential cross section is reproduced well by FR-method through eight orders of magnitude range

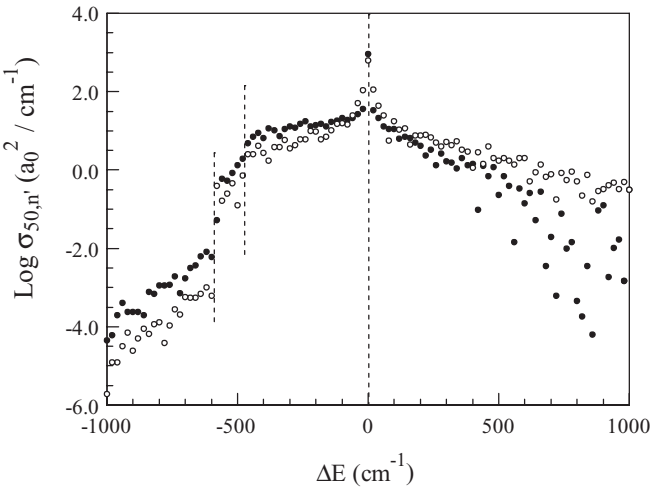

FIG. 4. Energy transfer function obtained by the original AR (filled symbols) and the developed FR (empty symbols) methods. The long dashed line at $\Delta E = 0$ separates quenching (to the left) from excitation (to the right). Purely vibrational quenching is to the left of the short dashed line at $\Delta E = -489\,\mathrm{cm}^{-1}$. Discontinuity at $\Delta E = -590\,\mathrm{cm}^{-1}$ is due to the vibrational mode character. Note that the FR method reproduces all these fine features. Initial ro-vibrational state is the same as in Figs. 1 and 3.

of values and in a broad range of ΔE. At large positive $\Delta E > +500\ \mathrm{cm}^{-1}$ the FR-method overestimates cross section (as discussed above), while at large negative $\Delta E < -500\ \mathrm{cm}^{-1}$ the FR-method somewhat underestimates the cross section. Note a sharp change of the slope at $\Delta E = -489\ \mathrm{cm}^{-1}$. This amount of energy corresponds to the initial rotational excitation of the molecule in this example, so, the point where the energy transfer function bends corresponds to transformation from the *ro-vibrational* quenching to purely *vibrational* quenching. Finally, note a discontinuity of cross section at $\Delta E = -590\ \mathrm{cm}^{-1}$. To the right of this dashed line the *normal-mode* state $n' = 47$ (which is $\sim 101\ \mathrm{cm}^{-1}$ below the initial state) participates in the energy transfer, while to the left of this line the energy transfer is dominated by the local-mode state (much smaller cross section, see below). Interestingly, even these fine features of the energy transfer function are reproduced by the FR-method.

C. Vibrational state-to-state transition cross sections

More detailed insight is provided by comparing cross sections for vibrational state-to-state transitions computed as

$$\sigma^{(i)}_{n,n'} = \frac{2\pi b_{\max}}{N} \sum b p^{(i)}_{n,n'}(b). \tag{19}$$

Here, the sum is over N trajectories in a batch and includes all the final (classical) rotational states. In this computational experiment we took, as initial states, four different rotational states of the normal-mode vibrational state $n = 51$, and four different rotational states of the local-mode vibrational state $n = 50$. Those are listed in Tables I and II. Total energies $E^{(i)}_n$ of these scattering resonances cover a broad range, from roughly $25\ \mathrm{cm}^{-1}$ to $630\ \mathrm{cm}^{-1}$ above dissociation threshold. Their widths $\Gamma^{(i)}_n$ (inversely proportional to lifetimes) also cover a broad range of values, 10^{-6} to $10^{-1}\ \mathrm{cm}^{-1}$. The final vibrational states are listed in the first column of Tables I and II.

The largest values in Tables I and II correspond to elastic scattering cross sections. They are all reproduced accurately enough for the normal-mode initial states (deviations are 11%-14%) and somewhat less accurately for the local-mode initial states (deviations are 2%-17%). Only in one case the deviation is quite large (39%, last column of Table II), but this is because this initial state is very close to the barrier top (large width of the resonance $\Gamma = 0.25\ \mathrm{cm}^{-1}$). It has short lifetime and, consequently, tends to dissociate. Small changes in the energy transfer lead to significant changes in the post-collisional behavior.

It is well known that the elastic scattering cross section, strictly speaking, diverges if the scattering motion is treated classically. Sometimes this problem is overcome by an appropriate choice of the maximum impact parameter, or by removing, in an *ad hoc* way,[42] the elastic scattering peak clearly seen at $\Delta E = 0$ in Fig. 3 (red) and Fig. 4 (dashed line). We tried several of these methods and saw very similar results. The elastic scattering cross sections given in Tables I and II were obtained by disregarding all trajectories with $|\Delta J| < 1$. This method allows removing selectively all points of the elastic scattering peak, without affecting the rest of data. Roughly, it corresponds to setting up the maximum impact parameter at $\sim 9\ a_0$ (see Fig. 3).

As for vibrationally inelastic processes, the largest cross sections are usually observed for transitions between states of same character. Normal-mode states tend to stabilize to the normal-mode states, while local-mode states tend to stabilize to proper local-mode states. For example, for the initial *normal-mode* state ($n = 51$) the largest inelastic cross section corresponds to the final state $n = 48$ (see Table I), which is the closest *normal-mode* state. Similarly, for the initial *local-mode* state ($n = 50$) the largest inelastic cross section corresponds to the final state $n = 47$ (see Table II), which is the closest *local-mode* state in the same dissociation channel. This qualitative feature is reproduced well by the FR method, but the absolute values of cross sections are different in the AR and FR cases. For the initial states at lower energies $E^{(i)}_n \leq 350\ \mathrm{cm}^{-1}$ the FR cross sections are a factor of $\times 2$ to $\times 5$ smaller, compared to the AR cross sections. This difference increases to $\times 8$ for states at higher energies $E^{(i)}_n \sim 420\ \mathrm{cm}^{-1}$ and $630\ \mathrm{cm}^{-1}$, respectively (last columns in Tables I and II).

Other entries in Tables I and II show similar differences of state-to-state cross sections obtained from AR and FR methods. Note that for smaller cross sections the statistical error is typically larger. In those cases when cross sections are reasonably large and statistical error is small (within ~25%) the typical difference between AR and FR results is $\times 4$. This is similar to performance of the rotationally sudden approximation in the time-independent methods, known to produce cross sections that are a factor of $\times 2$ to $\times 4$ smaller, compared to exact results.[43,44]

D. Stabilization cross sections

For approximate treatment of recombination kinetics at low and moderate pressure of M it is not really necessary to compute individual cross sections for all vibrational state-to-state transition. It is advantageous to introduce stabilization cross section for each scattering resonance:

$$\sigma^{(i)}_{n,stab} = \frac{2\pi b_{\max}}{N} \sum b P^{(i)}_{n,stab}(b), \tag{20}$$

$$P^{(i)}_{n,stab} = \sum_{E<0} p^{(i)}_{n,n'}. \tag{21}$$

The sum in Eq. (21) is over the final vibrational states below dissociation threshold, $E^{(i)}_n < 0$. Note that this energy includes the final rotational energy, so, the stabilization cross section characterizes the overall ro-vibrational quenching (within MQCT, where rotation is treated classically while vibration is treated with quantum mechanics). Stabilization cross sections are the most practically important moieties. Figure 5 shows convergence study of stabilization cross section for state $n = 50$ (same rotational state as before) in both AR and FR calculations. For a batch of 3000 trajectories the statistical error is rather small, typically close to 5%. Interestingly, Fig. 5 demonstrates that with only as few as 100 trajectories one can obtain a reasonable estimate of stabilization cross section.

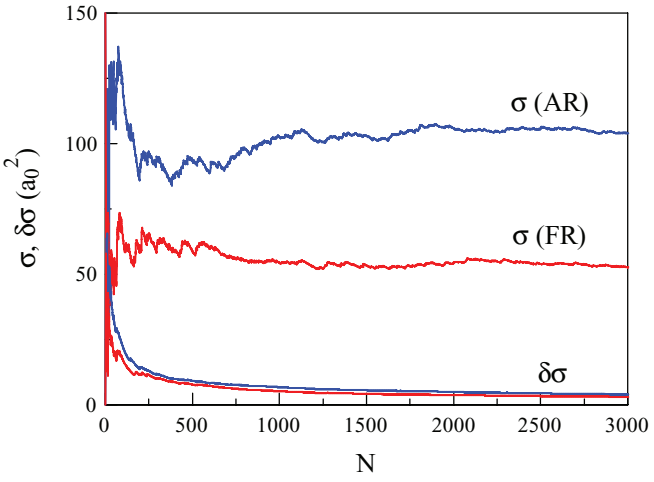

FIG. 5. Convergence of stabilization cross sections in the original AR (blue) and the developed FR methods (red). Statistical errors for each method are given at the bottom of the figure. Initial ro-vibrational state is the same as in Figs. 1, 3, and 4.

Last row in Tables I and II lists the values of stabilization cross sections for eight scattering resonances considered here. The values obtained from FR method are only a factor of $\times 2$ to $\times 3$ smaller, compared to AR method, in the entire range of rotational excitations and for both normal and local vibration mode states. This is very encouraging, since such a difference is usually assumed quite acceptable in most kinetics models. In Figure 6 we plotted the ratio of cross sections $\Re = \sigma_{\text{stab}}(\text{AR})/\sigma_{\text{stab}}(\text{FR})$ obtained from two methods, as a function of initial (total ro-vibrational) energy of the scattering resonance. Although the correlation is not particularly strong, these data suggest that a ratio of 2-to-3 is typical for the FR approach in the entire range of energies, when it is used to compute the ro-vibrational stabilization cross sections.

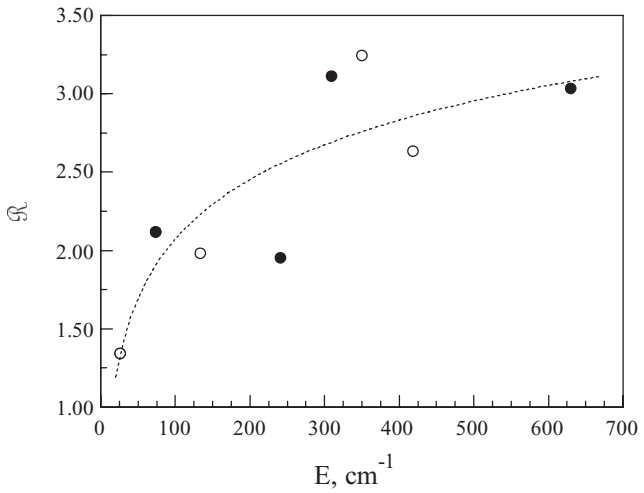

FIG. 6. Ratio of stabilization cross sections computed from the original AR method and the developed FR method. The data are presented for eight scattering resonances: four different rotational states of the normal mode vibrational state (filled symbols, see Table I) and four different rotational states of the local mode vibrational state (empty symbols, see Table II). The fit is by a logarithmic function.

V. CONCLUSION

In this paper we formulated the frozen-rotor approximation for MQCT and conducted a thorough numerical test to assess its efficiency and accuracy, in comparison to the original version of MQCT where rotation of the molecule in space is treated explicitly and adiabatically. The FR treatment of rotation only requires propagating a simple Eq. (17) with mean torque defined by Eq. (8), and computing the centrifugal potential function in Eq. (5), to add to the quantum Hamiltonian. This approach permits to block the artificial and undesirable ro-vibrational transitions at the pre- and post-collisional stages of the process. As for computational costs, the FR method is 3.8 times faster (for the 2D-model of ozone) because the backward propagation is no more needed and because the equations for rotational excitation/quenching become much simpler. Computational advantage of the FR approximation is expected to be more important in the case of full-dimensional 3D calculations of ozone stabilization, planned in the near future.

Although molecular orientation is fixed in space, the energy exchange between rotational, vibrational, and translational degrees of freedom still occurs in the FR method, allowing to compute ro-vibrational excitation and quenching. Noteworthy, behavior of the energy transfer function through eight orders of magnitude range of values and in a broad range of ΔE is reproduced well by the developed FR-method, including some fine features. In the range of moderate $-500 \leq \Delta E \leq +500$ cm^{-1} the FR-method is rather accurate. The absolute values of stabilization cross sections for scattering resonances trapped behind the centrifugal threshold are a factor 2-to-3 smaller (compared to the explicit-rotation approach). This performance is acceptable and is similar to the well-known sudden-rotation approximation in the time-independent inelastic scattering methods.

ACKNOWLEDGMENTS

Alexander Semenov (Marquette University) is gratefully acknowledged for fruitful discussions. This research was supported by the National Science Foundation (NSF) Atmospheric Chemistry Program, Division of Atmospheric Sciences, Grant No. 1252486. This research used resources of the National Energy Research Scientific Computing Center, which is supported by the Office of Science of the U.S. Department of Energy under Contract No. DE-AC02-05CH11231.

[1] C. Janssen, J. Guenther, K. Mauersberger, and D. Krankowsky, Phys. Chem. Chem. Phys. **3**, 4718 (2001).
[2] R. T Pack, R. B. Walker, and B. K. Kendrick, J. Chem. Phys. **109**, 6714 (1998).
[3] R. T Pack and R. B. Walker, J. Chem. Phys. **121**, 800 (2004).
[4] M. V. Ivanov, S. Yu. Grebenshchikov, and R. Schinke, J. Chem. Phys. **120**, 10015 (2004).
[5] K. Mauersberger, D. Krankowsky, C. Janssen, and R. Schinke, Adv. At., Mol., Opt. Phys. **50**, 1 (2005).
[6] Y. Q. Gao and R. A. Marcus, Science **293**, 259 (2001).
[7] D. Babikov, B. Kendrick, R. B. Walker, R. Schinke, and R. T Pack, Chem. Phys. Lett. **372**, 686 (2003).
[8] D. Babikov, B. Kendrick, R. B. Walker, and R. T Pack, J. Chem. Phys. **119**, 2577 (2003).

[9]D. Charlo and D. C. Clary, J. Chem. Phys. **117**, 1660 (2002).
[10]D. Charlo and D. C. Clary, J. Chem. Phys. **120**, 2700 (2004).
[11]T. Xie and J. M. Bowman, Chem. Phys. Lett. **412**, 131 (2005).
[12]M. V. Ivanov, S. Yu. Grebenshchikov, and R. Schinke, J. Chem. Phys. **130**, 174311 (2009).
[13]M. V. Ivanov and R. Schinke, Mol. Phys. **108**, 259 (2010).
[14]M. Ivanov and D. Babikov, J. Chem. Phys. **134**, 144107 (2011).
[15]M. Ivanov and D. Babikov, J. Chem. Phys. **136**, 184304 (2012).
[16]M. Ivanov and D. Babikov, "On molecular origin of mass-independent fractionation of oxygen isotopes in the ozone forming recombination reaction," Proc. Natl. Acad. Sci. U.S.A. (published online).
[17]L. Jiang and D. Babikov, Chem. Phys. Lett. **474**, 273 (2009).
[18]R. T Pack, J. Chem. Phys. **60**, 633 (1974).
[19]T. P. Tsien and R. T Pack, Chem. Phys. Lett. **6**, 54, 400 (1970).
[20]T. P. Tsien and R. T Pack, Chem. Phys. Lett. **8**, 579 (1971).
[21]T. P. Tsien, G. A. Parker, and R. T Pack, J. Chem. Phys. **59**, 5373 (1973).
[22]M. Sizun, F. Aguillon, V. Sidis, V. Zenevich, G. D. Billing, and N. Markovi, Chem. Phys. **209**, 327 (1996).
[23]F. Aguillon, V. Sidis, and J. P. Gauyacq, J. Chem. Phys. **95**, 1020 (1991).
[24]G. D. Billing, Comput. Phys. Rep. **1**, 239 (1984).
[25]G. S. Whittier and J. C. Light, J. Chem. Phys. **110**, 4280 (1999).
[26]D. Babikov, F. Aguillon, M. Sizun, and V. Sidis, Phys. Rev. A **59**, 330 (1999).
[27]G. D. Billing, *The Quantum Classical Theory* (Oxford University Press, New York, 2003).
[28]J. M. Bowman, Chem. Phys. Lett. **217**, 36 (1994).
[29]J. Qi and J. M. Bowman, J. Chem. Phys. **105**, 9884 (1996).
[30]J. Qi and J. M. Bowman, J. Chem. Phys. **107**, 9960 (1997).
[31]S. Carter and J. M. Bowman, J. Chem. Phys. **108**, 4397 (1998).
[32]S. Skokov and J. Bowman, J. Chem. Phys. **110**, 9789 (1999).
[33]S. Zou, S. Skokov, and J. M. Bowman, J. Phys. Chem. A **105**, 2423 (2001).
[34]R. Siebert, P. Fleurat-Lessard, R. Schinke, M. Bittererová, and S. C. Farantos, J. Chem. Phys. **116**, 9749 (2002).
[35]R. Prosmiti, S. C. Farantos, and H. S. Taylor, Mol. Phys. **82**, 1213 (1994).
[36]S. C. Farantos, D. Y. Lin, and H. Guo, Chem. Phys. Lett. **399**, 260 (2004).
[37]S. C. Farantos, Z. W. Qu, H. Zhu, and R. Schinke, Int. J. Bifurcation Chaos Appl. Sci. Eng. **16**, 1913 (2006).
[38]M. Ivanov and D. Babikov, Chem. Phys. Lett. **535**, 173 (2012).
[39]G. Lendvayt and G. C. Schatz, J. Phys. Chem. **96**, 3752 (1992); **98**, 6530 (1994).
[40]I. Oref and D. C. Tardy, Chem. Rev. **90**, 1407 (1990).
[41]M. Quack and J. Troe, "Gas kinetics and energy transfer," Chemical Society, London **2**, 175 (1977).
[42]M. Ivanov and D. Babikov, J. Chem. Phys. **134**, 174308 (2011).
[43]A. J. Banks, D. C. Clary, and H.-J. Werner, J. Chem. Phys. **84**, 3788 (1986).
[44]G. D. Billing and D. C. Clary, Chem. Phys. Lett. **90**, 27 (1982).